International Journal for Uncertainty Quantification, 1 (3): 257–278 (2011)

PINK NOISE, $1/f^{\alpha}$ NOISE, AND THEIR EFFECT ON SOLUTIONS OF DIFFERENTIAL EQUATIONS

Miro Stoyanov, Max Gunzburger, & John Burkardt*

Department of Scientific Computing, Florida State University, Tallahassee, Florida 32306-4120, USA

Original Manuscript Submitted: 27/02/2011; Final Draft Received: 31/03/2011

White noise is a very common way to account for randomness in the inputs to partial differential equations, especially in cases where little is know about those inputs. On the other hand, pink noise, or more generally, colored noise having a power spectrum that decays as $1/f^{\alpha}$, where f denotes the frequency and $\alpha \in (0, 2]$ has been found to accurately model many natural, social, economic, and other phenomena. Our goal in this paper is to study, in the context of simple linear and nonlinear two-point boundary-value problems, the effects of modeling random inputs as $1/f^{\alpha}$ random fields, including the white noise ($\alpha = 0$), pink noise ($\alpha = 1$), and brown noise ($\alpha = 2$) cases. We show how such random fields can be approximated so that they can be used in computer simulations. We then show that the solutions of the differential equations exhibit a strong dependence on α, indicating that further examination of how randomness in partial differential equations is modeled and simulated is warranted.

KEY WORDS: *random fields, colored noise, pink noise, stochastic finite element method*

1. INTRODUCTION

Given a subset $\mathcal{D} \in \mathbb{R}^d$ and/or an interval $\mathcal{I} \in \mathbb{R}$, a random field is a function of position and/or time whose value at any point $x \in \mathcal{D}$ and/or at any time $t \in \mathcal{I}$ is randomly selected according to an underlying probability density function (PDF), most often a Gaussian PDF. Here d denotes the spatial dimension. Thus a random field is expressed as $\eta(x, t; \omega)$ to indicate that the value of η not only depends on position and time, but also probabilistically on the associated PDF $\rho(\omega)$. Random fields come in two guises: uncorrelated and correlated, the former type commonly referred to as white noise, the latter as colored noise. Note that choosing the Gaussian PDF allows for a nonzero probability that the noise may, locally and momentarily, have an arbitrarily large modulus. Other choices for the PDF may be made, for example, a truncated Gaussian that excludes rare but large modulus samples or a simple uniform density over a finite interval. Also note that, for the most part, our discussion is made within the context of spatially dependent random fields, although it holds equally well for fields that instead, or in addition, depend on time.

A key concept used in this paper is that of the power spectrum or, synonymously, the energy spectral density associated with realizations of random fields. The power spectrum is a positive, real-valued function of the frequency f that gives the power, or energy density, carried by the field per unit frequency. Thus, the integral of the power density between two values of the frequency provide the amount of energy in the field corresponding to those frequencies. Mathematically speaking, the energy spectral density is the square of the magnitude of the continuous Fourier transform of the field.

The value of a white noise random field at any point is independent and uncorrelated from the values of that field at any other point. A white noise random field has a flat power spectrum, so that the energy of the field between the frequency values a and b depends only on $b - a$; thus, for example, there is just as much energy between the

*Correspond to Miro Stoyanov, E-mail: mksotyanov@gmail.com

2152–5080/11/$35.00

frequencies 1,000,100 and 1,000,200 as there is between the frequencies 100 and 200. It is obvious, then, that a white noise random field has infinite energy.

On the other hand, the value of a colored noise random field at any point may be independent but is correlated to the values of that field at other points; this explains, of course, why colored noise is also referred to as correlated noise. A particular class of colored noise fields has a power spectrum that decays as $1/f^\alpha$, where $\alpha \geq 0$ and f denotes the frequency. White noise corresponds to $\alpha = 0$, brown noise to $\alpha = 2$, and $\alpha = 1$ corresponds to pink noise. Pink noise has the property that the energy in the frequency interval $b - a$ depends only on b/a so that the energy between frequencies 10 and 20 is the same as that between frequencies 1,000,000 and 2,000,0000. Musically speaking, this means that all octaves have the same energy. For $\alpha \neq 1$, the energy in $1/f^\alpha$ noise grows as $f^{1-\alpha}$ so that it has infinite energy for $\alpha < 1$ and finite energy for $\alpha > 1$; thus, white noise, that is, the case $\alpha = 0$, has infinite energy. For pink noise, that is, for $\alpha = 1$, the energy grows as $\ln f$ so that it is also infinite. Figure 1 provides approximate realizations, determined using Algorithm 2 introduced in Section 2.2, of zero expectation $1/f^\alpha$ noise for $\alpha = 0$, 0.5, 1, 1.5, and 2 sampled at 1001 equally spaced points on the interval $[0, 1]$; for the three largest values of α, we plot two realizations. In practice, individual realizations are of no interest; rather, statistical information determined over many realizations is relevant. However, it is instructive to examine, as we do here, the effect that the choice of α has on realizations. Clearly, the random fields illustrated in Fig. 1 are very different, so that if one changes the input of a system from one of the fields to another, one can expect a large difference in the output of the system as well.

As α increases, the realizations of the noise become "smoother," illustrating the increasing correlation in the random field as α increases (see Fig. 1). The spatial average of the realizations also provides an inkling about the effect that increasing correlation can have on realizations. All fields illustrated in Fig. 1 are sampled from a standard Gaussian PDF, that is, the samples have zero expectation and unit variance. This implies, among many other things, that the expectation of the spatial average of the all five random fields vanishes. Of course, the spatial average of individual realizations do not, in general, vanish. In the white noise case, the sample at each point is uncorrelated from

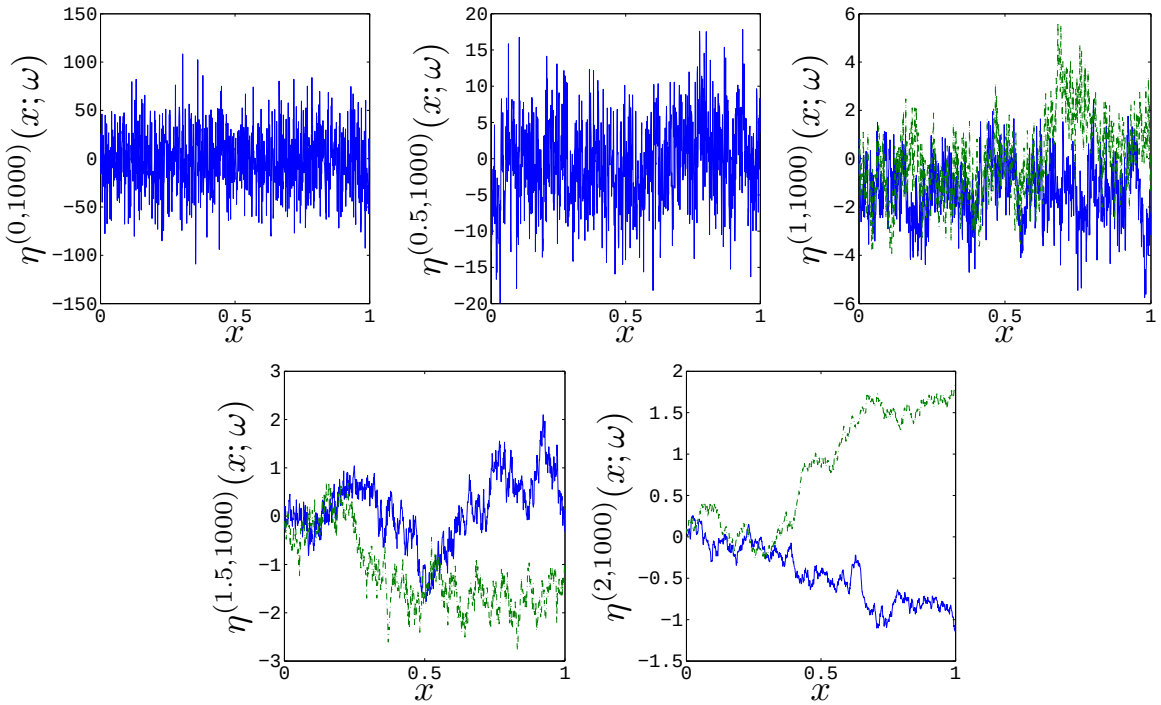

FIG. 1: Realizations of discretized $1/f^\alpha$ random fields with respect to a uniform grid having 1001 equally spaced points. Top row, left to right: $\alpha = 0$ (white noise), $\alpha = 0.5$, and $\alpha = 1$ (pink noise). Bottom row, left to right: $\alpha = 1.5$ and $\alpha = 2$ (brown noise).

the samples taken at other points, which results in a balance between the positive and negative samples so that the spatial average of individual realizations do tend to remain close to zero. As one increases the value of α, that balance can be increasingly upset so that the spatial average of an individual realization can be very different from zero. This is clearly seen in Fig. 1, where, in the brown noise case, for example, the spatial average is decidedly not zero.

$1/f^0$ noise is probably referred to as white noise because it contains all frequencies, much the same as white light contains all colors. Of course, the light spectrum is finite whereas the white noise spectrum, by definition, contains all frequencies equally. $1/f^2$ noise is called brown not because of any association with color, but because it corresponds to Brownian noise. A reason, but not the only one, suggested for referring to $1/f^1$ noise as pink noise is that brown noise is sometimes referred to as red noise and pink is "halfway" between white and red. Pink noise is also referred to as flicker noise because the noisy fluctuations, that is, the flicker, observed in signals from electronic devices is observed as having a $1/f$ power spectrum; flicker noise associated with vacuum tubes was studied some time ago, for example, [1–3].

White noise random fields are the most common, indeed, practically ubiquitous, model used in probabilistic methods for accounting for randomness in the inputs of systems governed by differential equations, especially for cases in which not much is known about the precise nature of the noise. This is not the case in many other settings, where instead pink noise, or more generally, $1/f^{\alpha}$ noise, is the model of choice. Pink noise and other $1/f^{\alpha}$ noise signals with $\alpha \neq 0$ or 2 have been observed in statistical analyses in astronomy, musical melodies, electronic devices, graphic equalizers, financial systems, DNA sequences, brain signals, heartbeat rhythms, psychological mental states, human auditory cognition, and natural images, just to name a few instances. Even fractals are intimately related to $1/f$ noise [4–6]; in fact, Mandelbrot's observation of the $1/f$ power spectrum of rainfall at different locations led to the development of the much more general fractal modeling of natural phenomena. See the website [7] for a very extensive bibliography for pink noise going back to the 1910s and the web articles [8, 9] for a discussion of the history, properties, and applications of $1/f^{\alpha}$ noise; see also the magazine article [10]. An especially illuminating treatment of $1/f^{\alpha}$ noise is given in [11]. The following quote from that paper is particularly telling (emphasis added here): "Scale invariance refers to the independence of the model from the scale of observation. The fact that $1/f$ noises (and Brownian motion) are scale invariant is suggested by their autospectral densities. If the frequency scale is changed, the original amplitude scaling can be obtained by simply multiplying by an appropriate constant. It was Mandelbrot's observation of the universality of scale invariance that led to this elevation as a fundamental property. *In fact, it can be argued that it is this property that is universal and accounts for the proliferation of power law noises throughout nature.*

Given that very often in actual measurements of fluctuations of signals in engineering, physical, chemical, biological, financial, medical, social, environmental, etc. systems, pink noise and not white noise is what is actually observed (it has even been suggested that $1/f$ noise is ubiquitous; see, for example, [12]) but on the other hand, in mathematical models of those systems the fluctuations are most often modeled as white noise, it is interesting to ask, Does it make any difference to the outputs of a system what type of noise one uses in the inputs to the system? The goal of this paper is to use the setting of a simple two-point boundary-value problem for ordinary differential equations to address this question, that is, to examine, in that simple setting, the differences in the statistical properties of solutions of differential equations having $1/f^{\alpha}$ random inputs for different values of α.

A random vector is a random field defined over a set of discrete points in space and/or time. Random vectors are of general interest, although for us, the interest is mostly their use in defining approximations to random fields defined over intervals. The power spectrum of a random vector is again a function of frequency determined by the square of the coefficients in the discrete Fourier transform of the vector.

Random fields can be defined by providing their expected value and covariance. For example, for a one-dimensional random field $\eta(x;\omega)$ in one spatial dimension, the mean and covariance are defined by

$$\mu(x) = \mathsf{E}\big[\eta(x;\omega)\big] = \int_{\Gamma} \eta(x;\omega)\rho(\omega)d\omega \qquad \text{and} \qquad \mathsf{Cov}(x,x') = \mathsf{E}\Big\{\big[\eta(x;\omega)-\mu(x)\big]\big[\eta(x';\omega)-\mu(x')\big]\Big\},$$

as well as, of course, the PDF $\rho(\omega)$; here Γ denotes the interval in $\mathbb{R}$ over which $\rho(\omega)$ is defined, e.g., for a Gaussian PDF, we have $\Gamma = (-\infty, \infty)$. Computing approximations to correlated random fields is relatively straightforward if one knows the expected value and covariance of the field. For example, a popular means for doing so is to determine

the (truncated) Karhunen-Loève expansion of the field [13, 14], something that can be accomplished by solving for the eigenvalues and eigenfunctions of the (discretized approximate) covariance function.

The covariances of white noise and brown noise (the expected value is usually assumed to be zero) are known; they are proportional to $\delta(x - x')$ and $\min(x, x')$, respectively, for random fields in one dimension. We can use the Karhunen-Loève expansion to determine approximate realizations of brown noise. Unfortunately, the covariance for $1/f^\alpha$ noise for α other than 0 or 2 is not directly defined; all one has to work with is knowledge about the power spectrum. White noise can be approximated using a sampling method over a discrete set of points. This is also possible for brown noise as well [see Eq. (13) and (16)]. In this paper we show how a similar method can be developed for general $1/f^\alpha$ noise.

2. GENERATING REALIZATIONS OF $1/f^\alpha$ RANDOM VECTORS AND FIELDS

In this section we study how to generate computable realizations of $1/f^\alpha$ random vectors and of approximations to $1/f^\alpha$ random fields.

2.1 Generating Realizations of $1/f^\alpha$ Random Vectors

We consider the algorithm of [11] for generating discrete $1/f^\alpha$ noise, that is, for generating $1/f^\alpha$ random vectors. Before we present that algorithm, we provide some motivation. We will use this algorithm as the basis for our approach toward approximating $1/f^\alpha$ random fields.

Let $w(x;\omega)$ denote a white noise random field. We define the random field $\xi(x;\omega)$ as the convolution of $w(x;\omega)$ with an impulse response function $h(x)$, that is,

$$\xi(x;\omega) = \int_0^x h(x-y)w(y;\omega)dy.$$

If $h^{(0)}(x) = \delta(x)$, where $\delta(x)$ denotes the Dirac delta function, the corresponding $\xi^{(0)}(x;\omega) = w(y;\omega)$, that is, we recover white noise. If instead,

$$h^{(2)}(x) = \begin{cases} 1 & \text{if } x \geq 0 \\ 0 & \text{if } x < 0, \end{cases}$$

we obtain $\xi^{(2)}(x;\omega)$ as a brown random field.

We proceed in a similar manner for infinite random vectors. Let $w_i(\omega)$, $i = 0, \ldots, \infty$ denote the components of an infinite causal white noise vector $\vec{w}(\omega)$, that is, the value of each $w_i(\omega)$ is sampled from a given PDF independently and uncorrelated from the value of any other component of $\vec{w}(\omega)$; we set $w_i(\omega) = 0$ for $i < 0$. We define the components of the infinite causal random vector $\vec{\xi}(\omega)$ through discrete convolution of $\vec{w}(\omega)$ with an infinite response vector $\vec{h}$, that is,

$$\xi_i(\omega) = \sum_{k=0}^{i} h_{i-k} w_k(\omega) \qquad \text{for } i = 0, \ldots, \infty. \tag{1}$$

If

$$h_i^{(0)} = \delta_i = \begin{cases} 1 & \text{if } i = 0 \\ 0 & \text{otherwise,} \end{cases} \tag{2}$$

the corresponding random vector $\vec{\xi}^{(0)}(\omega) = \vec{w}(\omega)$, that is, we recover the white random vector. If instead

$$h_i^{(2)} = \begin{cases} 1 & \text{for } i \geq 0 \\ 0 & \text{for } i < 0, \end{cases} \tag{3}$$

we obtain $\vec{\xi}^{(2)}(\omega)$ as a brown random vector.

We want to "interpolate" between $\vec{h}^{(0)}$ and $\vec{h}^{(2)}$ to obtain $\vec{h}^{(\alpha)}$ so that $\vec{\xi}^{(\alpha)}(\omega)$ is a $1/f^{\alpha}$ random vector. In order to obtain the correct power spectrum, we do the interpolation by first taking the Z transform [15] of $\vec{h}^{(0)}$ and $\vec{h}^{(2)}$ to obtain

$$H^{(0)}(z) = 1 \quad \text{and} \quad H^{(2)}(z) = \frac{1}{1 - z^{-1}}. \tag{4}$$

We then generalize to arbitrary $\alpha \in (0, 2)$ by setting

$$H^{(\alpha)}(z) = \frac{1}{(1 - z^{-1})^{\alpha/2}}. \tag{5}$$

Justification of this choice for the generalization of (2) and (3) is provided by demonstrating that it does indeed induce a random vector having a $1/f^{\alpha}$ power spectrum as is demonstrated in Section 2.1.1. Taking the inverse Z transform of (5), we obtain the vector $\vec{h}_{\alpha}$. To this end we represent $H^{(\alpha)}(z)$ as the power series

$$H^{(\alpha)}(z) = \sum_{j=0}^{\infty} H_j^{(\alpha)} z^{-j},$$

where

$$H_0^{(\alpha)} = 1 \qquad \text{and} \qquad H_j^{(\alpha)} = H_{j-1}^{(\alpha)} \frac{0.5\alpha + j - 1}{j} \quad \text{for } i = 1, 2, \ldots. \tag{6}$$

Then, the inverse Z transform of $H^{(\alpha)}(z)$ is given by the vector $\vec{h}^{(\alpha)}$ having components

$$h_i^{(\alpha)} = \sum_{j=0}^{\infty} H_j^{(\alpha)} \delta_{i-j} \qquad \text{for } j = 0, \ldots, \infty.$$

Substituting $h_i^{(\alpha)}$ into the discrete convolution (1), we obtain the infinite colored noise vector $\vec{\xi}^{(\alpha)}(\omega)$ having components

$$\xi_i^{(\alpha)}(\omega) = \sum_{k=0}^{i} \sum_{j=0}^{\infty} H_j^{(\alpha)} \delta_{i-k-j} w_k(\omega) = \sum_{j=0}^{\infty} H_j^{(\alpha)} \sum_{k=0}^{i} \delta_{i-k-j} w_k(\omega) = \sum_{j=0}^{\infty} H_j^{(\alpha)} w_{i-j}(\omega) \quad \text{for } i = 0, \ldots, \infty, \tag{7}$$

where $w_i(\omega)$ are the components of an infinite white noise vector and the weights $H_j^{(\alpha)}$ are determined by (6). Recall that we have set $w_i(\omega) = 0$ for $i < 0$, so that (7) reduces to

$$\xi_i^{(\alpha)}(\omega) = \sum_{j=0}^{i} H_j^{(\alpha)} w_{i-j}(\omega) \quad \text{for} \quad i = 0, \ldots, \infty. \tag{8}$$

A finite-dimensional colored noise M vector $\vec{\xi}^{(\alpha,M)}(\omega) \in \mathbb{R}^M$ is defined by selecting from (8) the first M components of the infinite noise vector $\vec{\xi}^{(\alpha)}(\omega)$ so that

$$\xi_i^{(\alpha,M)}(\omega) = \sum_{j=0}^{i} H_j^{(\alpha)} w_{i-j}(\omega) \quad \text{for} \quad i = 0, \ldots, M-1. \tag{9}$$

In matrix form (9) is given by

$$\vec{\xi}^{(\alpha,M)}(\omega) = \mathbf{H}^{(\alpha)} \, \vec{w}^{(\alpha,M)}(\omega)$$

where $\vec{w}^{(\alpha,M)}(\omega)$ is an M-dimensional white noise vector and $\mathbf{H}$ is the $M \times M$ unit lower triangular Toeplitz matrix given by

$$\mathbf{H}^{(\alpha)} = \begin{pmatrix} 1 & 0 & \cdots & & & 0 \\ H_1^{(\alpha)} & 1 & 0 & \cdots & & 0 \\ H_2^{(\alpha)} & H_1^{(\alpha)} & 1 & 0 & \cdots & 0 \\ \vdots & \vdots & \ddots & \ddots & & \vdots \\ \vdots & \vdots & & \ddots & \ddots & 0 \\ H_{M-1}^{(\alpha)} & H_{M-2}^{(\alpha)} & \cdots & \cdots & H_1^{(\alpha)} & 1 \end{pmatrix}.$$

Note that for white noise, $\mathbf{H}^{(0)} = \mathbf{I}$, the identity matrix, and for brown noise, all the entries on or below the main diagonal of $\mathbf{H}^{(2)}$ are equal to one. For $0 < \alpha < 2$ the subdiagonal entries of $\mathbf{H}^{(\alpha)}$ are all nonzero but monotonically decrease as one moves away from the main diagonal, that is, $1 > H_1^{(\alpha)} > H_2^{(\alpha)} > \cdots > H_{M-1}^{(\alpha)} > 0$ for $0 < \alpha < 2$. The rate of decrease accelerates as α decreases, which is an indication of the reduction in the correlation as α decreases.

The finite-dimensional colored noise vector $\vec{\xi}^{(\alpha,M)}(\omega)$ can be used to determine approximations of a $1/f^\alpha$ random field $\eta(x;\omega)$ (see Section 2.2).

We summarize the above discussion in the following algorithm that produces a realization of the discrete $1/f^\alpha$ noise vector $\vec{\xi}^{(\alpha,M)} \in \mathbb{R}^M$. Because discrete convolution has complexity $O(M^2)$, in the implementation of the above process we use, instead of the discrete convolution, the fast Fourier transform that has complexity of $O(M \log M)$. The implementation in [11] uses the real Fourier transform procedure given in [16]; we instead use the MATLAB complex fft() function.

Algorithm 1.
Given a positive integer M, $\alpha \in (0, 2]$, and the standard deviation σ of the zero-mean distribution from which the components w_i, $i = 0, \ldots, M-1$ of a white noise vector $\vec{w} \in \mathbb{R}^M$ are sampled. Then, the components ξ_j, $j = 0, \ldots, M-1$ of a discretized $1/f^\alpha$ random vector $\vec{\xi} \in \mathbb{R}^M$ are determined as follows:

- Determine the weight vector $\vec{H} \in \mathbb{R}^{2M}$ having components

$$H_j = \begin{cases} 1 & \text{for} \quad j = 0 \\ H_{j-1}\dfrac{0.5\alpha + j - 1}{j} & \text{for} \quad j = 1, \ldots, M-1 \\ 0 & \text{for} \quad j \geq M. \end{cases}$$

- Generate the vector $\vec{w} \in \mathbb{R}^{2M}$ whose components w_j, $j = 0, \ldots, M-1$ are independently sampled from a Gaussian distribution with zero mean and standard deviation σ and for which $w_j = 0$ for $j \geq M$.
- Using the fast Fourier transform algorithm, determine the discrete Fourier transforms $\widehat{\vec{H}} \in \mathbb{C}^{2M}$ and $\widehat{\vec{w}} \in \mathbb{C}^{2M}$ of $\vec{H}$ and $\vec{w}$, respectively.
- Set the components of the vector $\widehat{\vec{f}}_j \in \mathbb{C}^{2M}$ to the indexwise product $\widehat{f}_j = \widehat{h}_j \widehat{w}_j$ for $j = 0, \ldots, 2M-1$.
- Scale $\widehat{f}_0 = \frac{1}{2}\widehat{f}_0$ and $\hat{f}_M = \frac{1}{2}\widehat{f}_M$ and set $\widehat{f}_j = 0$ for $j > M$.
- Determine the vector $\vec{f} \in \mathbb{C}^{2M}$ as the inverse Fourier transform of $\widehat{\vec{f}}$.
- Then the components of the discretized $1/f^\alpha$ random vector $\vec{\xi} \in \mathbb{R}^M$ are given by

$$\xi_j = 2\Re(f_j) \quad \text{for} \quad j = 0, \ldots, M-1,$$

where the $\Re(\cdot)$ denotes the real part.

Note that Algorithm 1 produces Gaussian random vectors but that it can easily be changed so that it produces random vectors for other PDFs.

In the Appendix we provide the code for the MATLAB implementation of Algorithm 1. Variations of the code using uniform or truncated Gaussian distributions can be obtained at [17]. An implementation in C can be obtained at [18].

2.1.1 Verification of Algorithm for Generating Realizations of $1/f^{\alpha}$ Random Vectors

We now verify that Algorithm 1 does indeed produce random vectors with the desired $1/f^{\alpha}$ power spectrum, thus computationally justifying the generalization (5) of (4). We consider random vectors of size $M = 1000$ for five values of α, namely, $\alpha = 0$, 0.5, 1, 1.5, and 2. For each α we sample 10,000 realizations of the vector $\vec{\xi}^{(\alpha,1000)}$ determined by Algorithm 1. We determine the discrete Fourier transform of every realization of the noise vector and then compute the expected values of the squares of the real and imaginary parts of the (complex-valued) Fourier coefficients $\widehat{\xi}_k^{(\alpha,1000)}$ corresponding to the wave number k (which is, of course, the Fourier index and is proportional to the frequency.) These are plotted in Fig. 2, which, because the square of the Fourier coefficients are proportional to the energy density, is essentially a plot of the power spectrum. Note that the plots extend over only the wave numbers 1–500, because for real vectors such as $\vec{\xi}^{(\alpha,1000)}$, the Fourier coefficients occur in complex conjugate pairs. We also determine the power spectrum through a linear polynomial least-squares fit to $|\widehat{\xi}_k^{(\alpha,1000)}|^2$ as a function of the wave number k, that is, the sum of the squares of the real and imaginary parts of the Fourier coefficients plotted in Fig. 2. The slopes of the linear polynomial fits are given in Table 1. We include only the wave numbers from 1 to 400 in the least-squares fit because the accuracy of the Fourier coefficients deteriorates as the wave number increases. We observe that the power spectrum does indeed have the proper dependence on the wave number.

2.2 Generating Realizations of Approximate $1/f^{\alpha}$ Random Fields

We now show how to use the random vectors produced by Algorithm 1 to generate approximations of $1/f^{\alpha}$ random fields. In so doing, we ensure that the statistical properties of the approximations are largely independent of the number

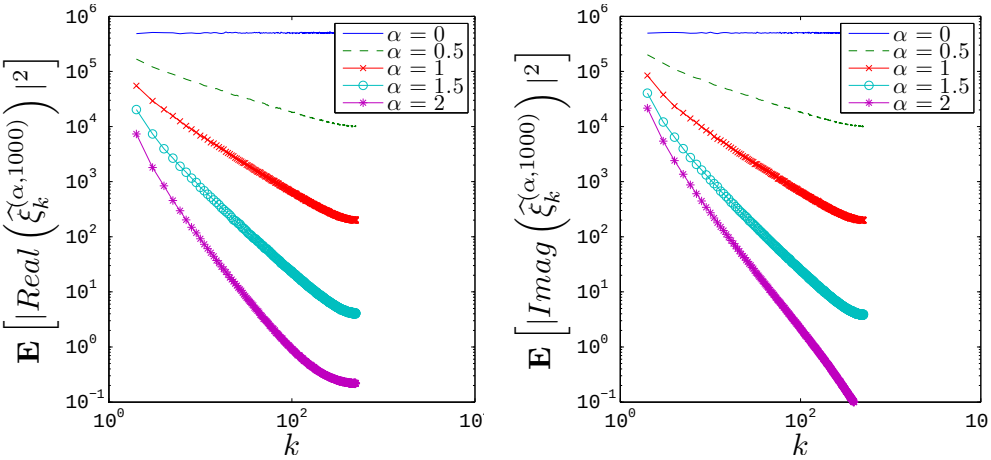

FIG. 2: For five values of α, plots of the expected values over 10,000 realizations of the square of the real (left) and imaginary (right) parts of the Fourier coefficients of the output of Algorithm 1 with $M = 1000$ plotted against the wave number.

TABLE 1: Slopes of the curves in Fig. 2 between wave numbers 1 and 400

α	0.0	0.5	1.0	1.5	2.0
Slope	0.002	−0.492	−0.990	−1.504	−1.958

of degrees of freedom used in the approximation. A necessary step for meeting this goal is a rescaling of the random vectors.

We consider the spatial domain $[0, L]$ which we subdivide into N equal intervals $I_j = (x_j, x_{j+1})$, $j = 0, \ldots, N-1$, where $x_j = j\Delta x$ with $\Delta x = L/N$. We use Algorithm 1 with $M = N$ to generate realizations of the discrete random vectors $\vec{\xi}^{(\alpha,N)}(\omega)$, whose components $\xi_j^{(\alpha,N)}(\omega)$, $j = 0, \ldots, N-1$ we associate with the interval I_j, $j = 0, \ldots, N-1$, respectively. (We note that often, especially when using finite difference methods for discretizing partial differential equations, random vectors are instead associated with grid points. See Section 3.1.1 for an example.) We then set

$$\eta^{(\alpha,N)}(x;\omega) = C_\alpha \sum_{j=0}^{N-1} \chi_j(x)\xi_j^{(\alpha,N)}(\omega), \tag{10}$$

where $\chi_j(x)$ denotes the characteristic function for the interval I_j. We want $\eta^{(\alpha,N)}(x;\omega)$ to approximate a $1/f^\alpha$ random field $\eta^{(\alpha)}(x;\omega)$. Note that because the components $\xi_j^{(\alpha,N)}(\omega)$ all have zero mean, we have, for any α, that

$$\mathsf{E}\big[\eta^{(\alpha,N)}(x;\omega)\big] = 0.$$

Thus we determine C_α by matching the variance of the approximate random field (10) to that of the corresponding random field $\eta^{(\alpha)}(x;\omega)$.

The variance of $\eta^{(\alpha,N)}(\omega)$ is given by

$$\begin{aligned}
\mathsf{E}\Big\{\big[\eta^{(\alpha,N)}(x;\omega)\big]^2\Big\} &= C_\alpha^2 \mathsf{E}\left[\sum_{j=0}^{N-1} \chi_j(x)\xi_j^{(\alpha,N)}(\omega) \sum_{k=0}^{N-1} \chi_k(x)\xi_k^{(\alpha,N)}(\omega)\right] \\
&= C_\alpha^2 \sum_{j=0}^{N-1}\sum_{k=0}^{N-1} \chi_j(x)\chi_k(x)\mathsf{E}\big[\xi_j^{(\alpha,N)}(\omega)\xi_k^{(\alpha,N)}(\omega)\big].
\end{aligned}$$

We have that

$$\chi_j(x)\chi_k(x) = \begin{cases} \chi_j(x) & \text{if } j = k \\ 0 & \text{if } j \neq k \end{cases}$$

so that

$$\mathsf{E}\Big\{\big[\eta^{(\alpha,N)}(x;\omega)\big]^2\Big\} = C_\alpha^2 \sum_{j=0}^{N-1} \chi_j(x)\mathsf{E}\Big\{\big[\xi_j^{(\alpha,N)}(\omega)\big]^2\Big\}. \tag{11}$$

We now try to match the result in (11) to the variance of the continuous random field $\eta^{(\alpha)}(x;\omega)$; we do so for white and brown random fields.

For a white random field, that is, for $\alpha = 0$, the variance of $\eta^{(0)}(x;\omega)$ is infinite; however, the integral of the variance over any finite spatial interval is finite and independent of the length of that interval, that is,

$$\int_x^{x+\Delta x} \mathsf{E}\Big\{\big[\eta^{(0)}(x;\omega)\big]^2\Big\} = \sigma^2. \tag{12}$$

For white noise, we have that the variance of the approximate random field $\eta^{(0,N)}(x;\omega)$ if given by

$$\mathsf{E}\Big\{\big[\eta^{(0,N)}(x;\omega)\big]^2\Big\} = C_0^2 \sum_{j=0}^{N-1} \chi_j(x)\mathsf{E}\Big\{\big[\xi_j^{(0,N)}(\omega)\big]^2\Big\} = C_0^2\sigma^2 \sum_{j=0}^{N-1} \chi_j(x) = C_0^2\sigma^2.$$

Then

$$\int_x^{x+\Delta x} \mathsf{E}\Big\{\big[\eta^{(0,N)}(x;\omega)\big]^2\Big\} = C_0^2\sigma^2\Delta x$$

so that comparing with (12), we have

$$C_0^2 = \frac{1}{\Delta x} = \frac{N}{L}$$

Thus for $\alpha = 0$, the approximation (10) of $\eta^{(0)}(x;\omega)$ is given by

$$\eta^{(0,N)}(x;\omega) = \frac{1}{\sqrt{\Delta x}} \sum_{j=0}^{N-1} \chi_j(x)\xi_j^{(0,N)}(\omega). \tag{13}$$

For a brown random field, that is, for $\alpha = 2$, the variance of $\eta^{(2)}(x;\omega)$ is given by

$$\mathsf{E}\Big\{ \big[\eta^{(2)}(x;\omega)\big]^2 \Big\} = \sigma^2 x \tag{14}$$

and the variance of the approximate random field $\eta^{(2,N)}(x;\omega)$ is given by

$$\mathsf{E}\Big\{ \big[\eta^{(2,N)}(x;\omega)\big]^2 \Big\} = C_2^2 \sum_{j=0}^{N-1} \chi_j(x)\mathsf{E}\Big\{ \big[\xi_j^{(2,N)}(\omega)\big]^2 \Big\} = C_2^2\sigma^2 \sum_{j=0}^{N-1} \chi_j(x)(j+1). \tag{15}$$

We interpret (15) as a piecewise constant approximation to (14) over the uniform partition of the interval $[0, L]$ into N subintervals of length $\Delta x = L/N$, in which case we see that

$$C_2^2 = \Delta x = \frac{L}{N},$$

so that for $\alpha = 2$, the approximation (10) of $\eta^{(2)}(x;\omega)$ is given by

$$\eta^{(2,N)}(x;\omega) = \sqrt{\Delta x} \sum_{j=0}^{N-1} \chi_j(x)\xi_j^{(2,N)}(\omega). \tag{16}$$

We generalize to $\alpha \in (0, 2)$ by "interpolating" between the values $C_0 = 1/\sqrt{\Delta x}$ for $\alpha = 0$ and $C_2 = \sqrt{\Delta x}$ for $\alpha = 2$ in the same manner as we did for the Z transform [see Eqs. (4) and (5)]. Thus we set

$$C_\alpha = (\Delta x)^{(\alpha-1)/2} \tag{17}$$

so that our approximation (10) of $\eta^{(\alpha)}(x;\omega)$ is given by

$$\eta^{(\alpha,N)}(x;\omega) = (\Delta x)^{(\alpha-1)/2} \sum_{j=0}^{N-1} \chi_j(x)\xi_j^{(\alpha,N)}(\omega). \tag{18}$$

Justifying this "interpolation" approach requires verification that the induced random fields do indeed have the expected $1/f^{\alpha}$ power spectra, which we do in Section 2.2.1.

We summarize the above discussion in the following algorithm that produces a realization of the approximate $1/f^{\alpha}$ random field $\eta^{(\alpha,N)}(x;\omega)$.

Algorithm 2.
Given the uniform subdivision of the interval $[0, L]$ into N subintervals I_j, $j = 0, \ldots, N-1$ of length $\Delta x = L/N$ and given the variance σ^2, the approximation $\eta^{(\alpha,N)}(x;\omega)$ is determined as follows:

- Use Algorithm 1 to generate a realization of the $1/f^{\alpha}$ random vector $\vec{\xi}^{(\alpha,N)}(\omega)$ based on sampling according to a given zero mean Gaussian PDF with variance σ^2.
- Set

$$\eta^{(\alpha,N)}(x;\omega) = (\Delta x)^{(\alpha-1)/2}\xi_j^{(\alpha,N)}(\omega) \quad \text{for} \quad x \in I_j, \;\; j = 0, \ldots, N-1.$$

Again, Algorithm 2 corresponds to Gaussian random fields, but again, it can be easily changed for random fields having other PDFs.

2.2.1 Verification of Algorithm 2 for Generating Realizations of Approximate $1/f^{\alpha}$ Random Fields

To verify that the approximate random field $\eta^{(\alpha,N)}(x;\omega)$ given in (18) [which is based on the choice for C_α made in (17)] is a good approximation to the $1/f^{\alpha}$ random field $\eta^{(\alpha)}(x;\omega)$, we examine its power spectrum. To this end we determine the Fourier cosine series for $\eta^{(\alpha,N)}(x;\omega)$, that is, we set

$$\eta^{(\alpha,N)}(x;\omega) = \sum_{k=0}^{\infty} \eta_k^{(\alpha,N)}(\omega)\cos(k\pi x),$$

where

$$\begin{aligned}
\eta_k^{(\alpha,N)}(\omega) &= \int_0^1 \eta^{(\alpha,N)}(x;\omega)\cos(k\pi x)dx = \int_0^1 (\Delta x)^{(\alpha-1)/2}\sum_{j=0}^{N-1}\chi_j(x)\xi_j^{(\alpha,N)}(\omega)\cos(k\pi x)dx \\
&= (\Delta x)^{(\alpha-1)/2}\sum_{j=0}^{N-1}\xi_j^{(\alpha,N)}(\omega)\int_0^1 \chi_j(x)\cos(k\pi x)dx = (\Delta x)^{(\alpha-1)/2}\sum_{j=0}^{N-1}\xi_j^{(\alpha,N)}(\omega)\int_{I_j}\cos(k\pi x)dx \\
&\approx (\Delta x)^{(\alpha+1)/2}\sum_{j=0}^{N-1}\xi_j^{(\alpha,N)}(\omega)\cos(k\pi x_j).
\end{aligned}$$

We set the number of intervals $N = 1000$ and use Algorithm 2 to determine 10,000 realizations of the approximate random field $\eta^{(\alpha,N)}(x;\omega)$ for each of five values of α. Those realizations are used to estimate the expected values of the first 1000 $|\eta_k^{(\alpha,N)}(\omega)|^2$, the square of the Fourier coefficients. In Fig. 3 these are plotted vs the wave number k. We also determine a linear least-squares fit to the first 800 values of $|\eta_k^{(\alpha,N)}(\omega)|^2$ to determine the slopes of the plots in Fig. 3. These are given in Table 2, where we see that the power spectrum of the approximate random field $\eta^{(\alpha,N)}(x;\omega)$ indeed has a $1/f^{\alpha}$ dependence.

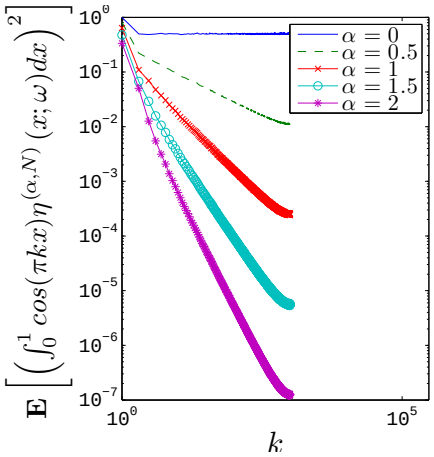

FIG. 3: For five values of α, plots of the expected values over 10,000 realizations of the square of the first 1000 Fourier coefficients of the approximate random field determined by Algorithm 2 plotted against the wave number. For this figure, $N = 1000$, $\sigma = 1$, and $L = 1$.

TABLE 2: Slopes of the curves in Fig. 3 between wave numbers 1 and 800

α	0.0	0.5	1.0	1.5	2.0
Slope	-0.004	-0.480	-0.959	-1.441	-1.927

Before providing further results about approximate $1/f^{\alpha}$ random fields generated by Algorithm 2, we clarify some notation we use because, so far, there has no ambiguity possible, but now there is. We, in fact, consider two types of averages, both of which involve integrals; integral averages with respect to the random variable ω, weighted by the PDF $\rho(\omega)$, are referred to as expected values, whereas averages with respect to the spatial variable x are referred to as spatial averages. Likewise, second moments with respect to ω are referred to as variances, whereas second moments with respect to x are referred to as energies. It is important to note that spatial averages and expected values commute, that is, the spatial average of an expected value is the same as the expected value of a spatial average. However, once even a single type of second moment is involved, statistical and spatial operations do not commute.

We consider the variance of the spatial average of the approximate random field $\eta^{(\alpha,N)}(x;\omega)$, that is, the variance of

$$\int_0^L \eta^{(\alpha,N)}(x;\omega)\,dx = \int_0^L (\Delta x)^{(\alpha-1)/2} \sum_{j=0}^{N-1} \chi_j(x)\xi_j^{(\alpha,N)}(\omega)\,dx = (\Delta x)^{(\alpha-1)/2} \sum_{j=0}^{N-1} \xi_j^{(\alpha,N)}(\omega) \left[\int_0^L \chi_j(x)\,dx\right]$$
$$= (\Delta x)^{(\alpha+1)/2} \sum_{j=0}^{N-1} \xi_j^{(\alpha,N)}(\omega). \tag{19}$$

Note that the expected value of the spatial average vanishes because the approximate random fields also have zero expected value at every point x. We use seven values for N ranging from 10 to 50,000 and, for each N, we generate a sample of size 10,000. The resulting statistics are given in Fig. 4, for which the Gaussian white noise samples are chosen to have unit variance. We observe that for a fixed value of σ in the Gaussian samples, the computed noise discretizations have statistical properties that differ appreciably as a function of α. Also, for fixed values of α, the statistics are largely insensitive to the value of the spatial discretization parameter N, that is, they are converging with increasing N.

We next consider the expected value of the "energy"

$$\int_0^L |\eta^{(\alpha,N)}(x;\omega)|^2 dx = (\Delta x)^{\alpha-1} \int_0^L \left[\sum_{i=0}^{N-1} \chi_i(x)\xi_i^{(\alpha,N)}(\omega) \sum_{j=0}^{N-1} \chi_j(x)\xi_j^{(\alpha,N)}(\omega)\right] dx$$
$$= (\Delta x)^{\alpha-1} \sum_{i=0}^{N-1}\sum_{j=0}^{N-1} \xi_i^{(\alpha,N)}(\omega)\xi_j^{(\alpha,N)}(\omega) \int_0^L \chi_i(x)\chi_j(x)dx$$
$$= (\Delta x)^{\alpha-1} \sum_{j=0}^{N-1} \left[\xi_j^{(\alpha,N)}(\omega)\right]^2 \int_0^L \chi_j(x)dx = (\Delta x)^{\alpha} \sum_{j=0}^{N-1} \left[\xi_j^{(\alpha,N)}(\omega)\right]^2.$$

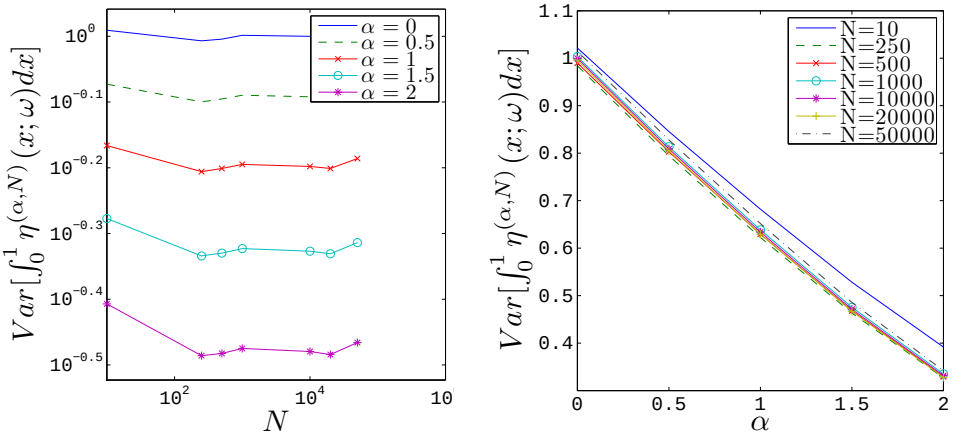

FIG. 4: For $\sigma = 1$ and $L = 1$, the variance of the spatial average of the piecewise constant approximate $1/f^{\alpha}$ random field $\eta^{(\alpha,N)}(x;\omega)$ given in (18) as a function of N (left) and α (right).

We use seven values for N and five values for α. For each pair (α, N), we generate 10,000 realizations of the approximate random field $\eta^{(\alpha,N)}(x;\omega)$ which we use to estimate the expected value of the energy. The results are given in Fig. 5. We see that for $\alpha < 1$, the expected value of the energy increases linearly with N but for $\alpha > 1$, it remains bounded and converges. For $\alpha = 1$, the expected value of the energy increases logarithmically. That can be seen from the linearity of the right plot in Fig. 5, which is a semi-log plot of the expected value of the energy vs. N for $\alpha = 1$; the slope of the that plot is approximately 0.095. Thus for $\alpha \leq 1$, a sequence of approximate $1/f^\alpha$ random fields having increasingly finer grid resolution will have an energy that grows unboundedly. Thus, the behavior of energy of the approximate random fields with respect to α mimics that of the random fields themselves.

3. DIFFERENTIAL EQUATIONS WITH $1/f^\alpha$ RANDOM FIELD INPUTS

In this section we consider differential equations having $1/f^\alpha$ random fields appearing in source or coefficient functions. Our goal is to study how the value of α in such random inputs affects statistical properties of the solutions of the differential equations.

3.1 Linear Two-Point Boundary Value Problem with $1/f^\alpha$ Source Term

We consider the two-point boundary value problem

$$-\frac{d^2}{dx^2}u^{(\alpha)}(x;\omega) = \eta^{(\alpha)}(x;\omega) \quad \text{for } x \in (0,1), \qquad u(0) = 0, \qquad u(1) = 0, \tag{20}$$

where $\eta^{(\alpha)}(x;\omega)$ is a $1/f^\alpha$ random field. The solution $u^{(\alpha)}(x;\omega)$ of (20) is itself a random field. How the statistical properties of that field are affected by the choice for α is what is of interest here.

In order to define a computational method for solving (20), we again use the uniform partition of the interval $[0,1]$ into the N subintervals I_j, $j = 0,\ldots,N-1$ of length $\Delta x = 1/N$ and also use the computable approximation $\eta^{(\alpha,N)}(x;\omega)$ given in (18) of the random field $\eta^{(\alpha)}(x;\omega)$. We seek a piecewise linear finite element approximation $u^{(\alpha,N)}(x;\omega)$ of the solution $u^{(\alpha)}(x;\omega)$ of (20), that is, an approximate solution of the form

$$u^{(\alpha,N)}(x;\omega) = \sum_{j=0}^{N} u_j^{(\alpha,N)}(\omega)\phi_j(x), \tag{21}$$

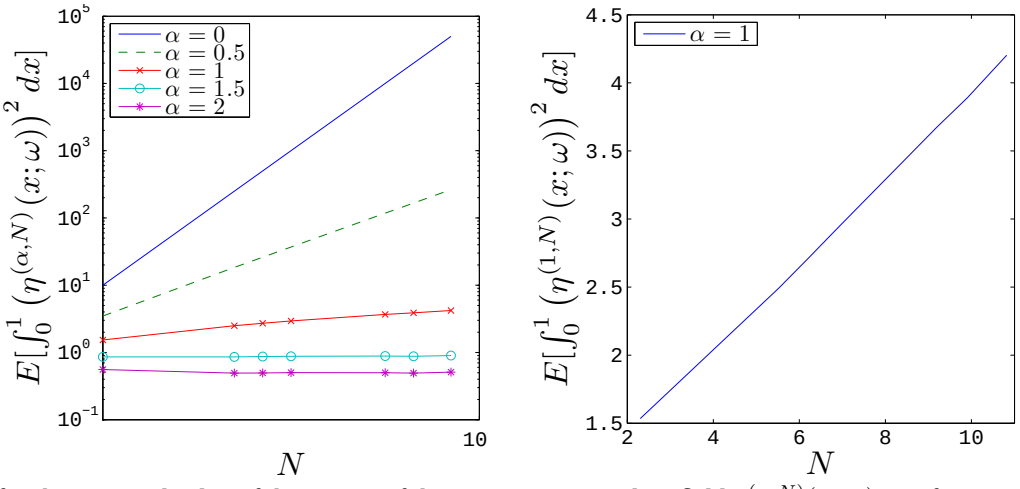

FIG. 5: Left: The expected value of the energy of the approximate random field $\eta^{(\alpha,N)}(x;\omega)$ as a function of α and N. Right: The expected value of the energy of the approximate pink noise random field $\eta^{(1,N)}(x;\omega)$ as a function of N.

where $\phi_j(x)$, $j = 0, 1, \ldots, N$ denote the usual piecewise linear hat functions corresponding to the partition of the interval $[0, 1]$ into the subintervals I_j, $j = 0, \ldots, N$. Then, setting $u_0^{(\alpha,N)}(\omega) = 0$ and $u_N^{(\alpha,N)}(\omega) = 0$, the standard Galerkin method results in the linear system

$$\frac{-u_{j-1}^{(\alpha,N)}(\omega) + 2u_j^{(\alpha,N)}(\omega) - u_{j+1}^{(\alpha,N)}(\omega)}{(\Delta x)^2} = (\Delta x)^{(\alpha-1)/2}\left[\frac{\xi_{j-1}^{(\alpha,N)}(\omega) + \xi_j^{(\alpha,N)}(\omega)}{2}\right] \quad \text{for } j = 1, \ldots, N-1 \tag{22}$$

from which the unknown nodal values $u_j^{(\alpha,N)}(\omega)$, $j = 1, \ldots, N-1$, of $u^{(\alpha,N)}(x;\omega)$ are determined. In (22), $\xi_j^{(\alpha,N)}(\omega)$, $j = 0, \ldots, N-1$ denote the components of the random vector $\vec{\xi}^{(\alpha,N)}(\omega)$ determined by Algorithm 1.

For given α, we use Algorithm 1 to generate a realization of the vector $\vec{\xi}^{(\alpha,N)}(\omega)$ and then solve the linear system (22) to generate the corresponding approximation $u^{(\alpha,N)}(x;\omega)$ of the solution of (20). Realizations of $u^{(\alpha,N)}(x;\omega)$ for five values of α and for $N = 1000$ are given in Fig. 6. Comparing with Fig. 1 that provides plots of realizations of the input $\eta^{(\alpha,N)}(x;\omega)$, we see that as one expects for elliptic equations, the solution is considerably smoother than the input [19].

Because the expected value of the $1/f^{\alpha}$ random field $\eta^{(\alpha)}(x;\omega)$ vanishes for all $x \in [0, L]$, it is easy to see, from the linearity of the differential operator and from the boundary conditions in (20), that the expected value of the solution $u^{(\alpha)}(x;\omega)$ vanishes as well. As a result, the expected value of the spatial average of $u^{(\alpha)}(x;\omega)$ also vanishes. Likewise, the linearity of the discrete system (22), the fact that $u_0^{(\alpha,N)}(\omega) = u_N^{(\alpha,N)}(\omega) = 0$, and the fact that the expected value of each $\xi_j^{(\alpha,N)}(\omega)$ vanishes imply that for all $j = 1, \ldots, N-1$, the expected value of $u_j^{(\alpha,N)}(\omega)$, $j = 1, \ldots, N-1$ vanishes as well, as does the expected value of the finite element approximation $u^{(\alpha,N)}(x;\omega)$ for

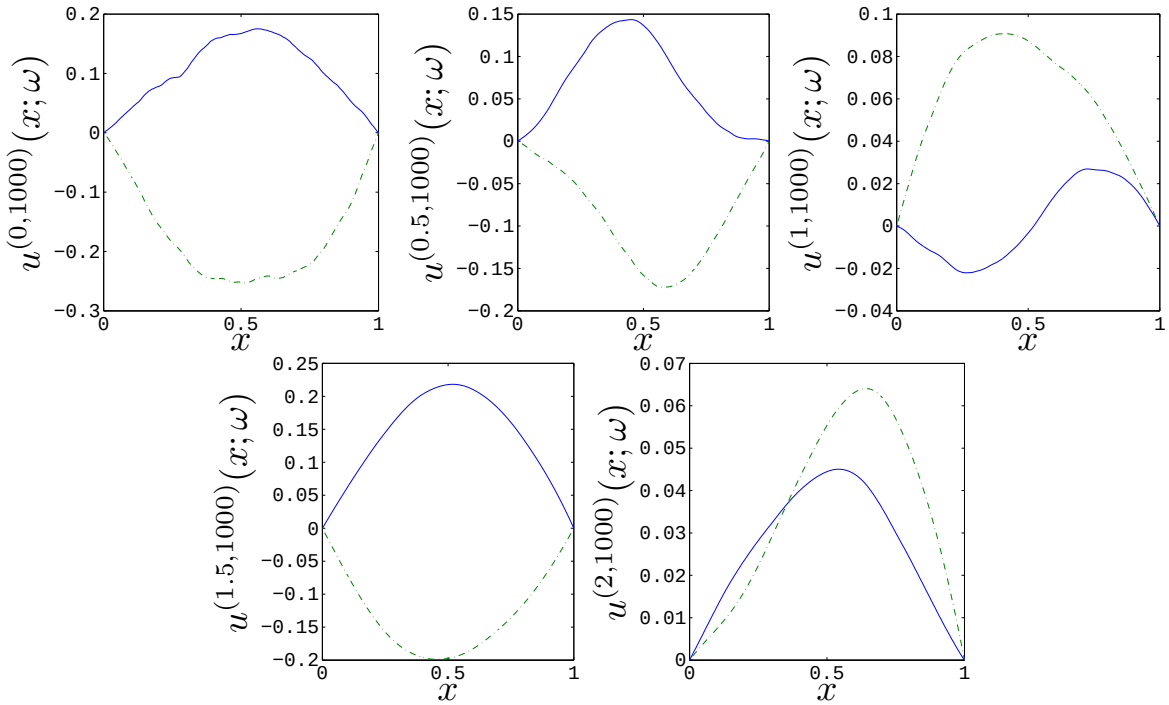

FIG. 6: Pairs of realizations of the approximation $u^{(\alpha,N)}(x;\omega)$, determined from Eqs. (21) and (22), to the solution of (20) for a uniform grid having $N = 1000$ subintervals and for $\sigma = 1$. Top row, left to right: $\alpha = 0$ (white noise input), $\alpha = 0.5$, and $\alpha = 1$ (pink noise input). Bottom row, left to right: $\alpha = 1.5$ and $\alpha = 2$ (brown noise input).

all $x \in [0, L]$. This holds true for the spatial average of $u^{(\alpha,N)}(x;\omega)$. Thus to study the effects that the choice of α have on the statistics of the approximate solution $u^{(\alpha,N)}(x;\omega)$, we examine the variance of the spatial average of that solution.

For each of several values of α and N we use Algorithm 1 to sample 10,000 realizations of the the $1/f^\alpha$ random vector $\vec{\xi}^{(\alpha,N)}(\omega)$ which we then use to compute, from Eq. (22), 10,000 realizations of the finite element approximation $u^{(\alpha,N)}(x;\omega)$ of the solution of Eq. (20). We then compute the variance of the spatial average of the approximate solutions. The results are given in Fig. 7. From that figure we observe the convergence with respect to increasing N and, more important, the strong linear dependence on the value of α.

It is natural to ask if by somehow "tweaking" the variance of the samples from which the input vector $\vec{\xi}^{(\alpha,N)}(\omega)$ is determined one can have the variance of the spatial average of $u^{(\alpha)}(x;\omega)$, or more relevant in practice, of its approximation $u^{(\alpha,N)}(x;\omega)$, independent of the value of α. This is indeed possible (see Section 3.2 for further discussion). However, other statistical properties, for example, the power spectrum, of $u^{(\alpha,N)}(x;\omega)$ would still remain strongly α dependent. By definition, the power spectrum of the $1/f^\alpha$ random field $\eta^{(\alpha)}(x;\omega)$ decays as $1/f^\alpha$, where f denotes the frequency. It is also well known (see [19]) that the solution operator of an elliptic equation such as (20) effects two orders of smoothing on the data so that we expect the power spectrum of the solution $u^{(\alpha)}(x;\omega)$ to decay as $1/f^{\alpha+4}$.

We now verify that the power spectrum of the approximate solution $u^{(\alpha,N)}(x;\omega)$ does indeed behave in this manner. (Recall that we have already shown, in Section 2.2, that the approximate random field $\eta^{(\alpha,N)}(x;\omega)$ does indeed have, for the most part, a $1/f^\alpha$ power spectrum.) We apply the same process to $u^{(\alpha,N)}(x;\omega)$ that led to Fig. 3 and Table 2 for the approximate input random field $\eta^{(\alpha,N)}(x;\omega)$, except that because of the homogeneous boundary conditions in (20), we now use the Fourier sine series. The analogous results for $u^{(\alpha,N)}(x;\omega)$ are provided in the left plot of Fig. 8 and Table 3. Note that the power spectrum decays at a faster rate for high values of the wave number; this is mostly due to the smoothing caused by the right-hand side in (22), in which the input noise vector is averaged over two successive components. This is why, for Table 3, we computed the slopes of the curves in Fig. 8 using only the first 100 wave numbers. In any case, we clearly observe an approximate $1/f^{\alpha+4}$ decay in the power spectrum for the approximate solution $u^{(\alpha,N)}(x;\omega)$. Thus, that power spectrum is strongly dependent on the value of α.

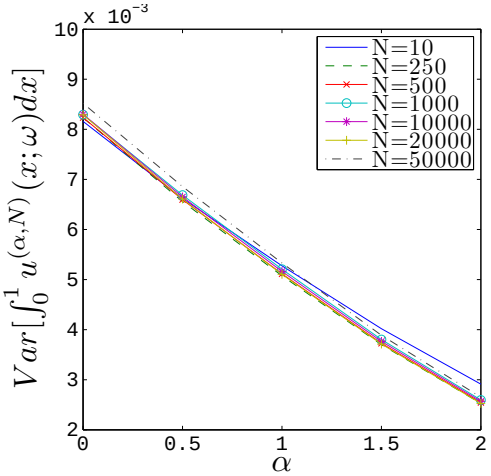

FIG. 7: The variance of the spatial average of the approximation $u^{(\alpha,N)}(x;\omega)$ determined from Eqs. (21) and (22) to the solution of (20) as a function of α and N for $\sigma = 1$.

TABLE 3: Slopes of the curves in the left plot in Fig. 8 between wave numbers 1 and 100

α	0.0	0.5	1.0	1.5	2.0
slope	-4.157	-4.661	-5.175	-5.715	-6.126

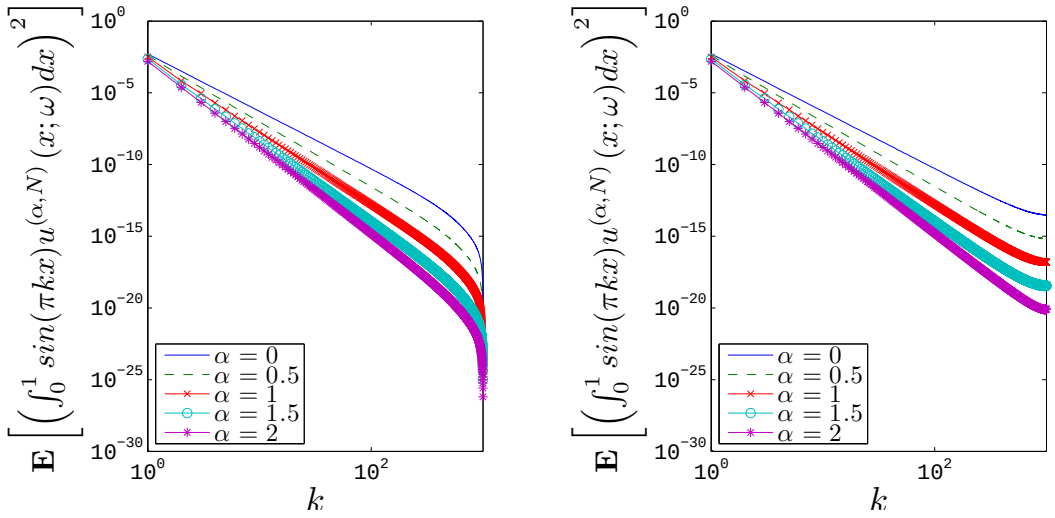

FIG. 8: For five values of α, plots of the expected values over 10,000 realizations of the square of the first 1000 Fourier coefficients of the finite element approximation (left) and finite difference approximation (right) of the solution of (20) plotted against the wave number. For this figure, $N = 1000$ and $\sigma = 1$.

3.1.1 Comparison with Finite Difference Discretizations

For comparison purposes, we briefly consider a standard finite difference approximation of the solution of (20). We use the same grid setup as used for the finite element discretization. We again have that $u_j^{(\alpha,N)}(\omega)$, $j = 0, \ldots, N$ denotes approximations of the nodal values of the exact solution of (20), that is, of $u_j^{(\alpha)}(x_j;\omega)$. Now, however, the components of the random input vector are associated with the $N-1$ interior grid nodes instead of grid intervals, that is, the components of the random vector $\vec{\xi}^{(\alpha,N-1)}(\omega)$ are associated with the of values $\eta^{(\alpha)}(x_j;\omega)$, $j = 1, \ldots, N-1$ of the random field $\eta^{(\alpha)}(x;\omega)$ evaluated at the interior grid points. Note that the same $(\Delta x)^{(\alpha-1)/2}$ scaling of the random vector is needed in the finite difference case.

The standard finite difference discretization of (20) leads to the linear system

$$\frac{-u_{j-1}^{(\alpha,N)}(\omega) + 2u_j^{(\alpha,N)}(\omega) - u_{j+1}^{(\alpha,N)}(\omega)}{(\Delta x)^2} = (\Delta x)^{(\alpha-1)/2}\xi_{j-1}^{(\alpha,N-1)}(\omega) \qquad \text{for } j = 1, \ldots, N-1 \tag{23}$$

along with $u_0^{(\alpha,N)}(\omega) = 0$ and $u_N^{(\alpha,N)}(\omega) = 0$. Comparing with (22), we see that the left-hand side is the same but that the right-hand side does not involve the averaging of neighboring components of the random vector $\vec{\xi}^{(\alpha,N-1)}(\omega)$. To see how this lack of averaging affects statistical properties of the approximate solution, we repeat the process that led to the left plot of Fig. 8 and Table 3 for the finite element case. For the finite difference case, the results are given in the right plot of Fig. 8 and Table 4. Comparing with the finite element results, we do not see any smoothing of the power spectrum at higher frequencies; in fact, we see a decrease in the rate of decay of the power spectrum. In Table 3, we again see the expected $1/f^{\alpha+4}$ power spectrum.

TABLE 4: Slopes of the curves in right plot of Fig. 8 between wave numbers 1 and 200

α	0.0	0.5	1.0	1.5	2.0
Slope	−3.938	−4.442	−4.957	−5.500	−5.968

3.2 Linear Two-Point Boundary Value Problem with Random Coefficients

Next we introduce noise into a coefficient of the Poisson problem. Consider the problem

$$\frac{d^2}{dx^2}u^{(\alpha)}(x;\omega) + \left[a + b\eta^{(\alpha)}(x;\omega)\right]u^{(\alpha)}(x;\omega) = 0 \quad \text{for} \quad x \in (0,1), \qquad u(0) = 0, \qquad u(1) = 1 \tag{24}$$

with $a = (4.5\pi)^2$ and $b = (\pi/2)^2$ and where $\eta^{(\alpha)}(x;\omega)$ denotes an $1/f^{\alpha}$ random field. Problems of this form arise in acoustics, for example, where case the coefficient denotes the square of the speed of sound. Of course, for such problems the coefficient should be positive, but here we consider (24) which has, if for example, $\eta^{(\alpha)}(x;\omega)$ denotes a Gaussian $1/f^{\alpha}$ random field, realizations with negative coefficient. The deterministic solution corresponding to $\eta^{(\alpha)}(x;\omega) = 0$ is given by $u_{\rm det}(x) = \sin(4.5\pi x)$.

In (24) we replace the random field $\eta^{(\alpha)}(x;\omega)$ by its approximation $\eta^{(\alpha,N)}(x;\omega)$ and then, as in Section 3.1, discretize via a finite element method based on piecewise linear polynomials, thus obtaining the linear system

$$\frac{u_{j-1}^{(\alpha,N)}(\omega) - 2u_j^{(\alpha,N)}(\omega) + u_{j+1}^{(\alpha,N)}(\omega)}{\Delta x} + \frac{\Delta x}{6}\Big\{\left[a + (\Delta x)^{(\alpha-1)/2}b\xi_{j-1}^{(\alpha,N)}(\omega)\right]\left[u_{j-1}^{(\alpha,N)}(\omega) + 2u_j^{(\alpha,N)}(\omega)\right]$$
$$+ \left[a + (\Delta x)^{(\alpha-1)/2}b\xi_j^{(\alpha,N)}(\omega)\right]\left[u_{j+1}^{(\alpha,N)}(\omega) + 2u_j^{(\alpha,N)}(\omega)\right]\Big\} = 0 \quad \text{for} \quad j = 1,\ldots,N-1 \tag{25}$$

along with $u_0^{(\alpha)}(\omega) = 0$ and $u_N^{(\alpha)}(\omega) = 1$.

We consider the difference $u^{(\alpha,N)}(x;\omega) - u_{\rm det}(x)$ between the approximate solution and the deterministic solution. Realizations of that difference for five values of α and for $N = 1000$ are given in Fig. 9. We then compute

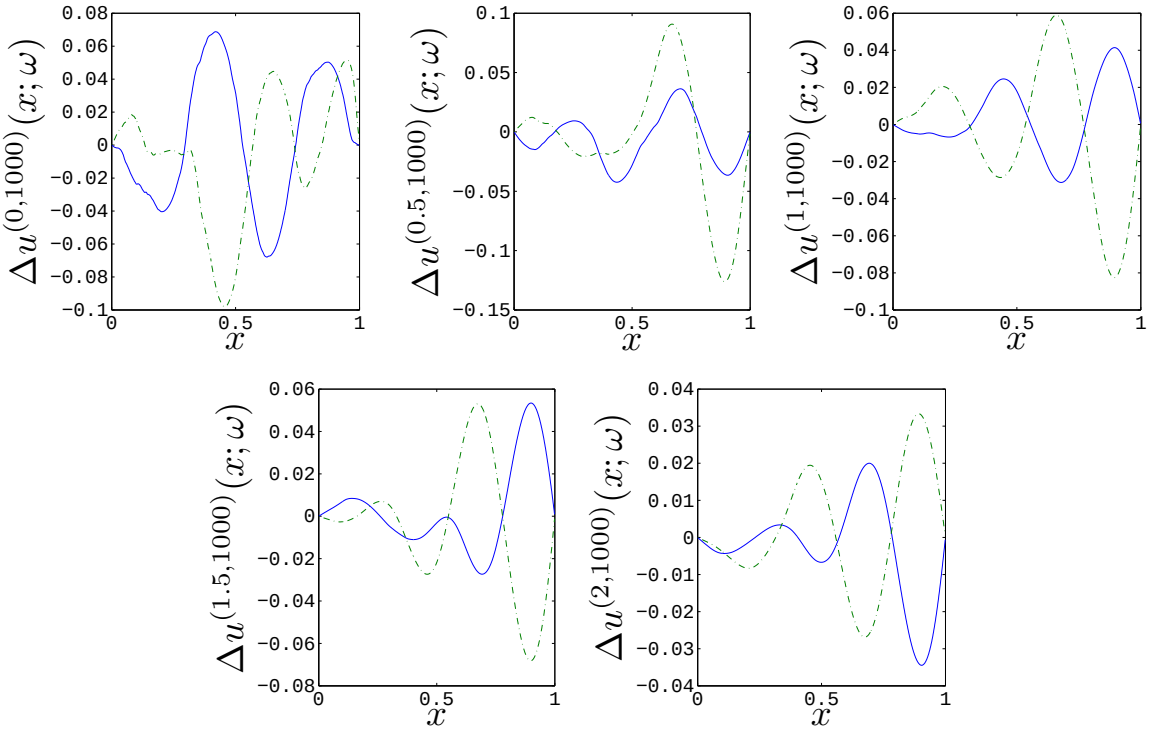

FIG. 9: Pairs of realizations of the deviation of the approximation $u^{(\alpha,N)}(x;\omega)$ to the solution of (24) from the deterministic solution for $N = 1000$ and $\sigma = 1$. Top row, left to right: $\alpha = 0$ (white noise input), $\alpha = 0.5$, and $\alpha = 1$ (pink noise input). Bottom row, left to right: $\alpha = 1.5$ and $\alpha = 2$ (brown noise input).

10,000 realizations for each α and different values of N and gather statistics. In particular, we determine the expected value and variance of $\int_0^1 \left[u^{(\alpha,N)}(x;\omega) - u_{\det}(x)\right]dx$ (see Fig. 10). We also provide, in Fig. 11, plots for the expected values of $\int_0^1 \left[u^{(\alpha,N)}(x;\omega) - u_{\det}(x)\right]^2 dx$. In all cases, a strong dependence on α and convergence with respect to N is observed. We also see, in Fig. 12, a dependence on α in the power spectrum of $u^{(\alpha,N)}(x;\omega) - u_{\det}(x)$.

In all of the examples so far, we chose $\sigma = 1$, that is, all random vectors were generated from an underlying standard normal distribution with variance 1. We can adjust the value of σ so that, for example, the quantities plotted in Fig. 11 match for different values of α. For example, if for $\alpha = 0$ we choose $\sigma_0 = 0.49$ and for $\alpha = 1$ we choose $\sigma = 1$, we have that

$$E\left\{\int_0^1 \left[u^{(0,N)}(x;\omega) - u_{\det}(x)\right]^2 dx\right\} = E\left\{\int_0^1 \left[u^{(1,N)}(x;\omega) - u_{\det}(x)\right]^2 dx\right\}. \tag{26}$$

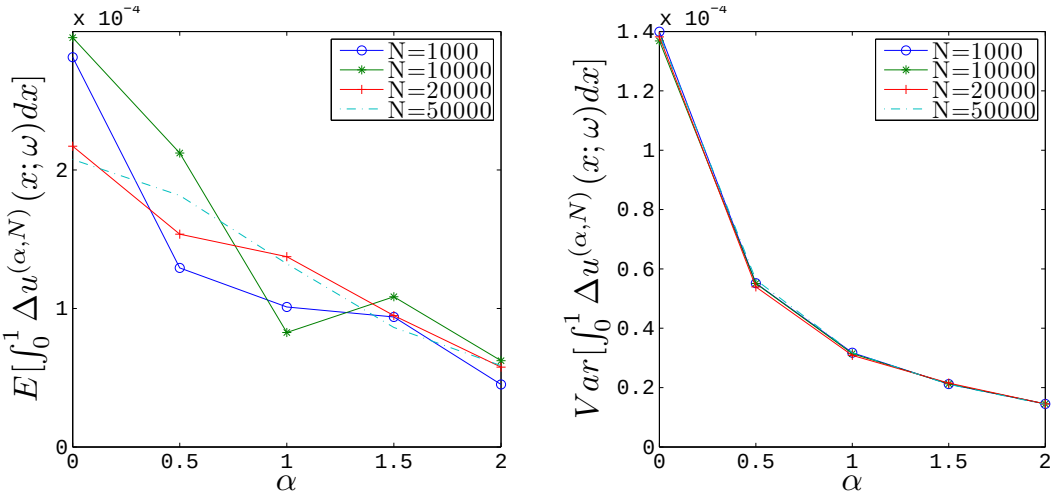

FIG. 10: Expected value (left) and variance (right) of $\int_0^1 \left[u^{(\alpha,N)}(x;\omega) - u_{\det}(x)\right]dx$ as a function of α and N for $\sigma = 1$.

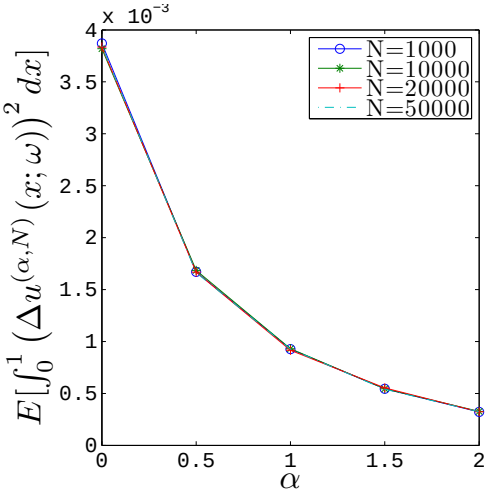

FIG. 11: Expected value of $\int_0^1 \left[u^{(\alpha,N)}(x;\omega) - u_{\det}(x)\right]^2 dx$ as a function of α and N for $\sigma = 1$.

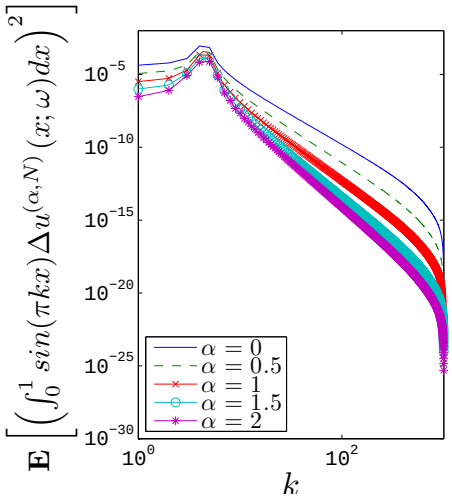

FIG. 12: For five values of α, plots of the expected values over 10,000 realizations of the square of the first 1000 Fourier coefficients of $u^{(\alpha,N)}(x;\omega) - u_{\rm det}(x)$ plotted against the wave number. Here, $N = 1000$ and $\sigma = 1$.

However, if we examine the power spectra for $u^{(0,N)}(x;\omega) - u_{\rm det}(x)$ and $u^{(1,N)}(x;\omega) - u_{\rm det}(x)$ given in Fig. 13, we see that the two spectra match only at frequencies with the highest energy density. The decay rate for higher and lower frequencies is quite different.

3.3 Nonlinear Two-Point Boundary Value Problem with Additive Noise

The final example we consider is the steady-state nonlinear Burgers equation

$$\mu\frac{d^2}{dx^2}u^{(\alpha,N)}(x;\omega) + \frac{1}{2}\frac{d}{dx}\left[u^{(\alpha,N)}(x;\omega)\right]^2 = 2\mu + 2x^3 + \eta^{(\alpha)}(x;\omega), \qquad u(0) = 0, \qquad u(1) = 1. \tag{27}$$

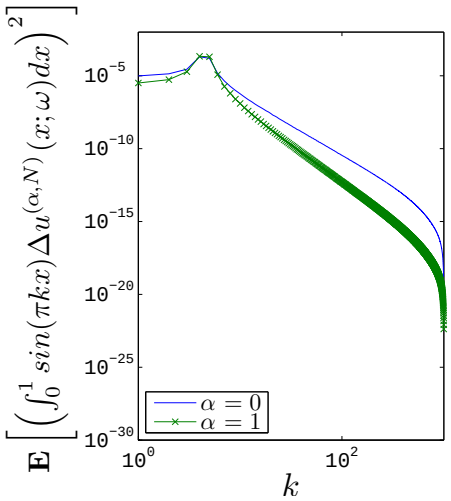

FIG. 13: For $(\sigma,\alpha) = (0.49, 0)$ and $(\sigma,\alpha) = (1,1)$, plots of the expected values over 10,000 realizations of the square of the first 1000 Fourier coefficients of $u^{(\alpha,N)}(x;\omega) - u_{\rm det}(x)$ plotted against the wave number. Here, $N = 1000$.

The exact noise-free solution is $u_{\text{det}}(x) = x^2$. We take $\mu = 0.1$ to increase the relative influence of the nonlinear term uu_x and set $\sigma = 1$. We obtain approximations of the solution $u(x;\omega)$ of (27) via a piecewise linear finite element method, resulting in

$$\mu\frac{u_{j-1}^{(\alpha,N)}(\omega) - 2u_j^{(\alpha,N)}(\omega) + u_{j+1}^{(\alpha,N)}(\omega)}{\Delta x} + \frac{\left[u_{j-1}^{(\alpha,N)}(\omega) - u_{j+1}^{(\alpha,N)}(\omega)\right]\left[u_{j-1}^{(\alpha,N)}(\omega) + u_j^{(\alpha,N)}(\omega) + u_{j+1}^{(\alpha,N)}(\omega)\right]}{6}$$

$$= (\Delta x)\left(2\mu - \frac{1}{3}x_{j-1}^3 - \frac{4}{3}x_j^3 - \frac{1}{3}x_{j+1}^3\right) + (\Delta x)^{(\alpha-1)/2}\left[\frac{\xi_{j-1}^{(\alpha,N)}(\omega) + \xi_j^{(\alpha,N)}(\omega)}{2}\right], \quad \text{for } j = 1,\ldots,N-1,$$

along with $u_0^{(\alpha,N)}(\omega) = 0$ and $u_N^{(\alpha,N)}(\omega) = 1$. This nonlinear system is solved via Newton's method, using the deterministic solution as an initial guess. Realizations of $u^{(\alpha,N)}(x;\omega) - u_{\text{det}}(x)$ for different values of α are given in Fig. 14. In Fig. 15 we provide the values for the variance of $\int_0^1 \left[u^{(\alpha,N)}(x;\omega) - u_{\text{det}}(x)\right]dx$ and the expected value of $\int_0^1 \left[u^{(\alpha,N)}(x;\omega) - u_{\text{det}}(x)\right]^2 dx$. Once again, we observe that the statistical properties of the solution of (27) have a strong dependence on α.

In Fig. 16, we also plot the power spectrum of $u^{(\alpha,N)}(x;\omega)$ for $N = 1000$ and for different values of α. We observe significant differences between the power spectra for $\alpha < 1$ and almost no differences for $\alpha > 1$. We also see this from the slopes of the least-squares fits given in Table 5.

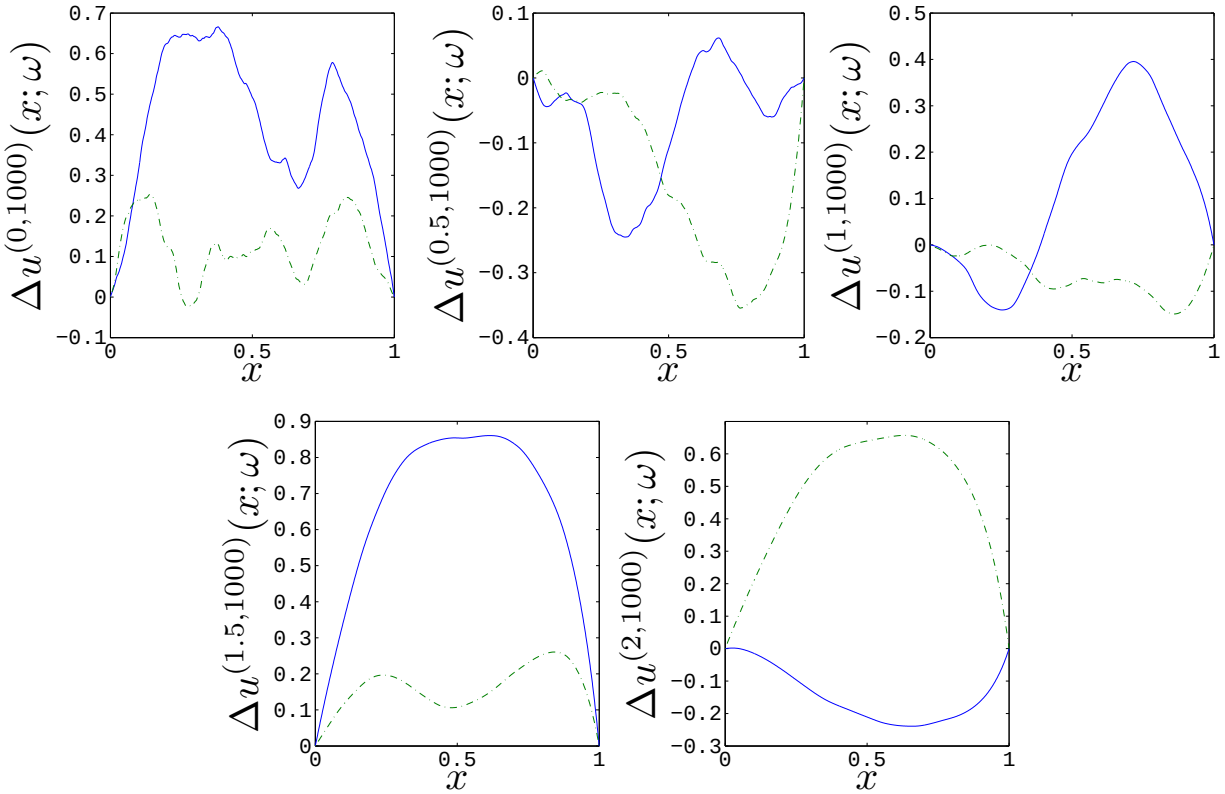

FIG. 14: Pairs of realizations of the approximation $u^{(\alpha,N)}(x;\omega)$ to the solution of (27) for a uniform grid having $N = 1000$ subintervals and for $\sigma = 1$ and $\mu = 0.1$. Top row, left to right: $\alpha = 0$ (white noise input), $\alpha = 0.5$, and $\alpha = 1$ (pink noise input). Bottom row, left to right: $\alpha = 1.5$ and $\alpha = 2$ (brown noise input).

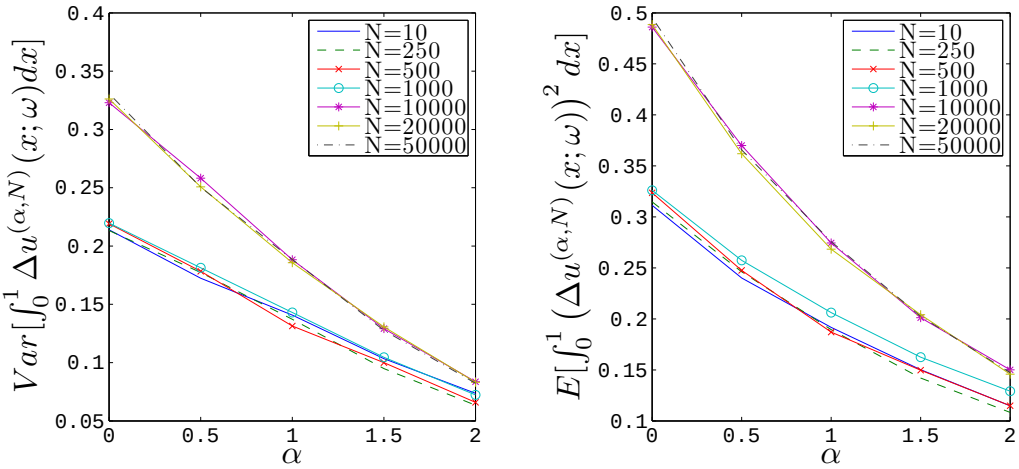

FIG. 15: The variance of $\int_0^1 \left[u^{(\alpha,N)}(x;\omega) - u_{\text{det}}(x)\right]dx$ (left) and the expected value of $\int_0^1 \left[u^{(\alpha,N)}(x;\omega) - u_{\text{det}}(x)\right]^2 dx$ for the Burger's equation example (27) with $\sigma = 1$ and $\mu = 0.1$.

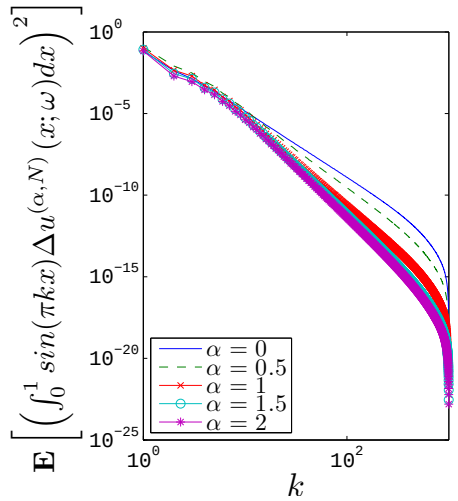

FIG. 16: For five values of α, plots of the expected values over 10,000 realizations of the square of the first 1000 Fourier coefficients of the difference between the approximate solution $u^{(\alpha,N)}(x;\omega)$ and the deterministic (noise free) solution of (27) plotted against the wave number; here, $N = 1{,}000$ and $\sigma = 1$.

TABLE 5: Slopes of the curves in Fig. 16 between wave numbers 1 and 400

α	0.0	0.5	1.0	1.5	2.0
Slope	-4.1495	-4.7176	-5.4171	-5.9465	-6.0076

4. CONCLUDING REMARKS

Whereas generating approximations of colored $1/f^\alpha$ noise is more expensive than that for white noise ($\alpha = 0$), we see that noise is used as inputs to differential equations, resulting in solutions with drastically different properties. Given that many natural, social, financial, and other phenomena are accurately modeled by $1/f^\alpha$ random fields and given that white noise remains the most popular means for modeling unknown random inputs in partial differential

equations, the differences the two have on the solution of the equations is worth considering. In this paper we attempted to illustrate and quantify these differences in admittedly simple settings that are meant to motivate further studies of the use of $1/f^{\alpha}$ noise in the context of partial differential equations.

For example, it is natural to consider the extension of our study to cases in which the spatial domain is multidimensional and in which there is time evolution as well. An immediate observation is that all the observations about approximating $1/f^{\alpha}$ over a spatial interval carry over unchanged to a one-dimensional time interval. If the domain is a product region of time and space, then standard Fourier transform methods allow us to construct a multidimensional noise function as the product of one-dimensional noise functions; the component noise functions, in turn, are each defined by a number of sample points N_i, a variance σ_i^2, and a value of α_i, which are then input to a multiple-FFT version of Algorithm 1. As far as the FFT computations are concerned, no distinction need be made between time and space dimensions. On the other hand, there may be good reasons to use different values of σ_t and α_t associated with the time-wise noise component from those used for the spatial components.

Some guidance in choosing the components of the noise parameters in two or higher space dimensions can be gained from considering the one-dimensional case. Suppose, for instance, that a three-dimensional spatial domain is being considered. Then the instantaneous energy of the noise signal, with parameters α_x, α_y, and α_z, will be the same as that for a noise signal over a one-dimensional region with parameter $\alpha = \sqrt{\alpha_x^2 + \alpha_y^2 + \alpha_z^2}$. In the common case where there is no directional preference for the noise in the spatial dimensions, it is natural to choose common values of σ_x^2 and α_x for all spatial noise components.

ACKNOWLEDGMENTS

This work was supported in part by the U.S. Air Force, Office of Scientific Research, under grant no. FA9550-08-1-0415.

APPENDIX: MATLAB CODE FOR ALGORITHM 1

We provide the code for the MATLAB implementation of Algorithm 1. Note that because MATLAB does not allow for zero indices, we have shifted the indices by one. An implementation in C can be obtained at [18].

```
function [ xi ] = f_alpha ( m, sigma, alpha )
  hfa = zeros ( 2 * m, 1 );
  hfa(1) = 1.0;
  for j = 2 : m
    hfa(j) = hfa(j-1) * ( 0.5 * alpha + ( j - 2 ) ) / ( j - 1 );
  end
  hfa(m+1:2*m) = 0.0;
  wfa = [ sigma * randn( m, 1 ); zeros( m, 1 ); ];
  [ fh ] = fft( hfa );
  [ fw ] = fft( wfa );
  fh = fh( 1:m + 1 );
  fw = fw( 1:m + 1 );
  fw = fh .* fw;
  fw(1)       = fw(1) / 2;
  fw(end)     = fw(end) / 2;
  fw = [ fw; zeros(m-1,1); ];
  xi = ifft( fw );
  xi = 2*real( xi(1:m) );
end
```

REFERENCES

1. Johnson, J., The Schottky effect in low frequency circuits, *Phys. Rev.*, 26:71–85, 1925.
2. Schottky, W., Small-shot effect and flicker effect, *Phys. Rev.*, 28:74–103, 1926.

3. Orfanidis, S., *Introduction to Signal Processing*, Prentice-Hall, Englewood Cliffs, NJ, 1995.
4. Mandelbrot, B., Some noises with l/f spectrum and a bridge between direct current and white noise, *IEEE Trans. Inf. Theory*, 13:289, 1967.
5. Mandelbrot, B. and Van Ness, J., Fractional Brownian motions, fractional noises and applications, *SIAM Rev.*, 10:422, 1968.
6. Mandelbrot, B., *The Fractal Geometry of Nature*, Freeman, San Francisco, 1982.
7. Li, W., *A Bibliograph on* $1/f$ *Noise*, http://www.nslij-genetics.org/wli/1fnoise/.
8. Ward, L. and Greenwood, P., 1/f noise, *Scholarpedia*, 2:1537, 2007, http://www.scholarpedia.org/article/1/f_noise.
9. *Wikipedia*, Pink noise, http://en.wikipedia.org/wiki/Pink_noise.
10. Gardner, M., White and brown music, fractal curves and one-over-f fluctuations, *Sci. Am.*, 238(4):16–32, 1978.
11. Kasdin, J., Discrete simulation of colored noise and stochastic processes and $1/f^{\alpha}$ power law noise generation, *Proc. IEEE*, 83:802–827, 1995.
12. Bak, P., Tang, C., and Wiesenfeld, K., Self-organized criticality: An explanation of $1/f$ noise, *Phys. Rev. Lett.*, 59:381–384, 1987.
13. Karhunen, K., Über lineare Methoden in der Wahrscheinlichkeitsrechnung, *Ann. Acad. Sci. Fennicae. Ser. A. I. Math.-Phys.*, 37:1–79, 1947.
14. Loève, M., *Probability Theory*, Springer-Verlag, New York, 1978.
15. Jury, E. I., *Theory and Application of the Z-Transform Method*, Krieger Publishing Co., Malabar, FL, 1973.
16. Press, W., Flannery, B., Teukolsky, S., and Vertterling, W., *Numerical Recipes*, Cambridge University Press, Cambridge, MA, 1986.
17. Implementation of Algorithm 1 written in MATLAB, http://people.sc.fsu.edu/∼jburkardt/m_src/cnoise/cnoise.html
18. Implementation of Algorithm 1 written in C, http://people.sc.fsu.edu/∼jburkardt/c_src/cnoise/cnoise.html
19. Evans, L. C., *Partial Differential Equations, Graduate Studies in Mathematics*, Vol. 19, American Mathemetical Society, Providence, RI, 1998.